On the Effect of Blockage Objects in Dense MIMO SWIPT Networks

Ayse Ipek Akin, *Student Member, IEEE*, Ivan Stupia, *Member, IEEE*, and Luc Vandendorpe, *Fellow, IEEE*

***Abstract*— Simultaneous wireless information and power transfer (SWIPT) is characterized by the ambiguous role of multi-user interference. In short, the beneficial effect of multi-user interference on RF energy harvesting is obtained at the price of a reduced link capacity, thus originating nontrivial tradeoffs between the achievable information rate and the harvestable energy. Arguably, in indoor environments, this tradeoff might be affected by the propagation loss due to blockage objects like walls. Hence, a couple of fundamental questions arise. How much must the network elements be densified to counteract the blockage attenuation? Is blockage always detrimental on the achievable rate-energy tradeoff? In this paper, we analyze the performance of an indoor multiple-input multiple-output SWIPT-enabled network in the attempt to shed a light of those questions. The effects of the obstacles are examined with the help of a stochastic geometry approach in which the locations of energy sources (also referred to as power heads) are distributed by using a Poisson point process and walls are generated through a Manhattan Poisson line process. The stochastic behavior of the signal attenuation and the multi-user interference is studied to obtain the joint complementary cumulative distribution function of information rate and harvested power. Theoretical results are validated through Monte Carlo simulations. Eventually, the rate-energy tradeoff is presented as a function of the density of walls to emphasize the cross-dependences between the deployment of the network elements and the macro parameters characterizing the topology of the venue.**

***Index Terms*— Simultaneous wireless information and power transfer (SWIPT), stochastic geometry, indoor environment, Manhattan Poisson line process, blockage modeling.**

I. Introduction

A. Background and Motivations

SIMULTANEOUS wireless information and power transfer (SWIPT) is an emerging concept promoted to increase the battery life of low power wireless devices. The main idea behind SWIPT is to use the same signal to transfer information and power simultaneously. The trade-off achievable between harvested energy and information rate in a single SWIPT link was originally presented by Varshney in [1]. Few years later, Zhang and Ho [2] showed the benefits of multi-input multi-output (MIMO) techniques on the performance of the SWIPT link with practical receiver architectures.

At the network level, an interesting aspect of SWIPT systems is the ambivalent role of the multi-user interference (MUI). Traditionally, MUI is considered as an undesired factor for wireless information transfer (WIT) due to the detrimental effect on the coverage probability and the information rate [3], [4]. On the contrary, for wireless power transfer (WPT), the interference can be used as an additional source of energy to be harvested [5], [6]. It is therefore doubtless that interference may have a major impact in determining the achievable rate-energy trade-off in SWIPT-enabled networks. MUI is even more crucial when the constraints on the minimum received power imposed by the current RF harvesting technologies (tens of microwatts) are considered. These constraints, together with the limitations on RF emissions for guaranteeing the public safety, suggest that the deployment of SWIPT power heads (PHs) must be denser than that of traditional access points in wireless networks, thus increasing the role played by MUI on system performance.

Another consequence of the network elements' densification is that the rate-energy trade-off is likely to be highly dependent on the spatial locations of the network elements, especially in indoor environments where the effect of the blocking objects is highly correlated in space. Therefore, idealised network models, like the Wyner model and the regular hexagonal or square grid models (see [7], [8]), are inadequate to describe the correlation structure of shadowing, since they rely on specific PHs deployments. Zhang *et al.* [9] propose an analytically tractable model for handling the effect of walls in indoor environments by making use of a stochastic geometry approach [10]. In this model, the plane is divided into rooms of random sizes to mimic the obvious circumstance that more users are likely to appear in larger rooms than in smaller rooms. Finally, as mentioned in [3], a stochastic geometry approach circumvents the possible concerns regarding the repeatability and the transparency of Monte Carlo simulations. Moreover, stochastic geometry revealed itself as useful tool to analyze the performance of SWIPT-enabled relay networks [11], ad-hoc networks [12], sensor networks [13] and cellular networks [14], [15].

Though the methodology that is presented in [14] and [15] is extremely valuable in providing a tool for analyzing the performance of stochastic SWIPT-enabled networks, these studies consider an outdoor cellular network that is too sparse to satisfy the constraints on the minimum received power that

Manuscript received December 21, 2017; revised May 4, 2018 and August 24, 2018; accepted October 9, 2018. Date of publication October 16, 2018; date of current version February 14, 2019. This work was supported by F.R.S.-FNRS under the EOS program (EOS project 30452698), by INNOVIRIS under the COPINE-IOT project and by UCL under the ARC SWIPT project. The associate editor coordinating the review of this paper and approving it for publication was Y. Li. *(Corresponding author: Ayse Ipek Akin).*

The authors are with the Institute of Information and Communication Technologies, Electronics and Applied Mathematics, Université catholique de Louvain, 1348 Louvain-la-Neuve, Belgium (e-mail: ayse.akin@uclouvain.be).

Color versions of one or more of the figures in this paper are available online at http://ieeexplore.ieee.org.

Digital Object Identifier 10.1109/TCOMM.2018.2876308

would enable RF energy harvesting. Moreover, both papers consider distance-based path-loss functions only, thus failing in describing the correlated structure of the signal blockage due to buildings and walls. In this perspective, along with the already mentioned work [9], other relevant contributions in this field have been presented in [16] and [17]. Bai *et al.* [16] have proposed a mathematical framework to model blockages with random sizes, locations, and orientations in cellular networks using concepts from random shape theory. In [17], a generative model based on stochastic geometry is developed to analyze the shadowing effect in urban environments. This work has been extended to in-building systems in [9] by modeling the walls' distribution as a Manhattan Poisson Line Process (MPLP). It is worth mentioning that the assumption behind this work is that the blockage-based penetration loss is the dominant factor and free-space propagation loss can be neglected. This model, while convenient for traditional data communication networks, conflicts with the typical operating conditions of SWIPT systems, in which the minimum received energy must be in the order of few microwatts to enable RF harvesting, so that a small difference on the distance can have a huge impact on the achievable rate-energy trade-off. More realistically, Müller *et al.* [18] jointly considered distance-dependent path-loss, wall blockage and small-scale fading in information-only wireless networks and examined the average number of blockages for several wall generation methods, from random shape theory to semi-deterministic and heuristic approaches. In this study, they considered different fixed transmitter configurations that provide the best scenario with respect to the interference. The conclusions of this interesting work show that MPLP wall generation yields the tightest lower bound with respect to the signal-to-interference ratio (SIR) results among all the mathematically tractable wall generation methods. To the best of our knowledge, for SWIPT-enabled indoor networks, there has not been any study showing the effect of the obstacles combined with distance-dependent path-loss.

B. Novelty and Contributions

All these concerns motivate us to propose a stochastic geometry analysis for dense in-building MIMO power-splitted SWIPT networks. MPLP is considered for the distribution of the walls while the PHs are randomly distributed on the plane as a Poisson Point Process (PPP). As a channel model, distance dependent path-loss, blockage-based path-loss and fast fading are considered. In order to study the trade-off between information rate and harvested power, an analytical expression of the Joint Complementary Cumulative Distribution Function (J-CCDF) is derived by jointly considering the effects of obstacles, distance and multiple antennas. Eventually, our mathematical framework is validated through Monte Carlo simulations.

The main contributions of this paper can therefore be summarized as follows:

- In contrast to prior contributions relevant to SWIPT, [14], [15], we consider the effect of randomly located blockage objects like walls. This is of particular importance for any scenario accounting for the realistic levels of power enabling RF harvesting.
- Differently from [9], we consider the joint effect of the distance dependent propagation loss and the blockages for a SWIPT-enabled network. Moreover, the locations of both PHs and walls are modeled through a stochastic process. This allows a macro-level investigation of the interactions between the network and the venue in which it is deployed.
- Müller *et al.* [18] consider an information-only scenario. More significantly, they assume that the positions of the transmitters are fixed and known a priori. In our manuscript, both the positions of the PHs and of the walls are modeled as Poisson processes. It follows that the characterization of multi-user interference depends on the density of PHs as well as on the density of blocking objects. This model allows a multi-dimensional analysis in which the impact of both the network densification and the density of blocking objects on the rate-energy trade-offs are jointly analyzed.
- An analytical expression of the cumulative distribution function of the multi-user interference as a function of the density of walls is provided. A similar result is also obtained for the distribution of the minimum propagation loss.
- The reported numerical results provide important insights on the interplay between the network and the in-building environment from the perspective of the rate-energy trade-off. We clarify the role of the SWIPT receiver architecture when an ultra-dense deployment of the network elements is considered. The potential performance improvements that can be achieved by means of maximum ratio transmission (MRT)-maximum ratio combining (MRC) MIMO techniques are also assessed.

The rest of this paper is organized as follows. Section II describes the system and path-loss model. We focus on performance analyses in Section III. In Section IV, numerical results are presented and finally the paper is concluded in Section V.

Notation: $j = \sqrt{-1}$ denotes the imaginary unit. $\mathbb{E}(\cdot)$ is the expectation operator. $\mathbb{1}\{\cdot\}$ is the indicator function. $\mathrm{Im}\{\cdot\}$ denotes the imaginary part. $\Gamma(\cdot\,,\cdot)$ is the upper-incomplete Gamma function [19, eq. 8.350.2]. ${}_pF_q(a_1, ..., a_p; b_1, ..., b_q; \cdot)$ is the generalized hypergeometric function [19, eq. 9.14.1]. $\mathcal{H}(\cdot)$ denotes the Heaviside function and $\bar{\mathcal{H}}(\cdot) = 1 - \mathcal{H}(\cdot)$.

II. System Model

In this section, we first introduce the major elements constituting the MIMO SWIPT network investigated in this paper. Then, some blanket assumptions on the spatial distribution of both the network elements and the blockage objects are made clear. For illustrative purposes, an instance of an indoor SWIPT network over a large area is shown in Fig.1, where the lines represent walls and the markers symbolize PHs. It is worth recalling that this paper targets a stochastic characterization of the SWIPT performance for a generic low power device (LPD) equipped with a power splitting receiver.

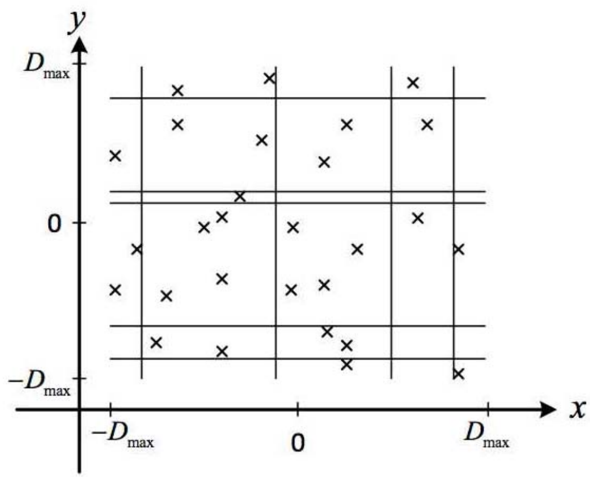

Fig. 1. One realization of the MPL and PP processes.

A. SWIPT Enabled Indoor Model

We consider a MIMO SWIPT network deployed in a two-dimensional indoor area. The SWIPT waveforms are generated by a set of randomly deployed PHs each equipped with n_t antennas. The LPD embedding a SWIPT receiver with n_r antennas is located at the center of the investigated region. It is assumed that the data delivered to the LPD comes from the PH providing the minimum average signal attenuation. In order to increase the performance of the information transfer process, the received signals captured from the different LPD antennas are processed using MRC, while MRT is implemented at the transmitter side. The technical challenges that might appear in a practical implementation of MRT with such a limited amount of energy available are extremely large. Just to mention a few, the imperfect knowledge of the estimated SINR, the temporal variations of the propagation environment for LPD with low duty cycle, and so forth. All these important issues are however out of the scope of this paper whose objective is to evaluate the potentiality of MRT-MRC processing in improving the rate-energy trade-off of the link. The SWIPT receiver operates according to the power splitting (PS) scheme: the received signal is split in two streams of different power levels by using a power splitting ratio ρ, where $0 \leq \rho \leq 1$. While one signal stream is sent to the rectenna circuit for energy harvesting, the other stream is used for information decoding. The power wirelessly delivered in the downlink can then be used for enabling all the LPD functionalities, including subsequent uplink communications. Hence, provided that a reliable energy consumption model for the LPD is available, the rate-energy trade-off also defines the operating conditions (e.g. data rates, duty cycles, etc.) in the uplink that can be supported through SWIPT.

B. Signal Propagation

Similarly to what has been done in [18], we assume that the signals are subject to distance dependent path-loss, wall blockages and small scale fading. The path-loss and the wall blockages are jointly modeled through the following log-distance dependent law:

$$l_N(r) = \begin{cases} \dfrac{\kappa r^{\beta}}{K^N} & \text{if } r \geq \kappa^{-1/\beta} \\ 1 & \text{otherwise} \end{cases} \tag{1}$$

where r is the distance between the PH and the device, β is the path-loss exponent, $K \in [0, 1)$ is the so called penetration loss, and N is a random variable representing the number of walls between a generic PH and the device. The path-loss constant is defined as $\kappa = (\frac{4\pi}{v})^2$, where $v = c_0/f_c$ is the transmission wavelength, f_c and c_0 being the carrier frequency (Hz) and the speed of light (m/sec), respectively. The small scale fading is modeled through random variables following a Rayleigh distribution to account for the multi-path propagation effect. More accurate fading models, like shadowed $\kappa-\mu$, can be adopted. However, using those models would harm the readability of the analytical results without bringing any additional insights into the spatially correlated structure of the blocking effect. Hence, in this paper, we focus on the more tractable Rayleigh fading model.

C. Spatial Distribution of PHs

For analyzing an ultra-dense MIMO SWIPT network in an indoor environment, we capitalize on a stochastic geometry approach. To achieve this, the possible sets of PHs deployed in a given area are modeled as instances of a homogeneous PPP Ψ of density λ_{PH}. Under the assumption of large indoor network, [9], thanks to the Slivnyak-Mecke's theorem [10, Th. 1.4.5] we will obtain a statistical characterization of the performance metrics for a typical LPD which is located at the origin of the $x-$ and $y-$ axes. This assumption is justified by the ultra-dense scenario considered, i.e. $\frac{1}{\lambda_{PH}} \ll \pi R_D^2$, where R_D is the maximum distance at which a PH's contribution to the global interference has a non-negligible impact on the achievable rate-energy trade-offs. As already mentioned, we assume that the information transfer towards the typical LPD is guaranteed by the PH ensuring the smallest average signal attenuation, also referred to as serving PH. From the information transfer perspective the other PHs are considered as interferers. The set of interfering PHs is denoted by $\Psi^{(\backslash 0)}$.

D. Random Wall Placement

Differently from previous studies (e.g. [15]), this paper focuses on an indoor environment. It follows that our signal propagation model must comprise wall blockages. Again, we adopt a stochastic approach in which the positions of walls are modeled as Manhattan Poisson Line Processes (MPLP). Generally speaking, MPLP is used to generate random lines in an Euclidean space $\mathbb{R}^n$. For the 2-D case, this is achieved by defining two homogeneous PPPs $\Psi_x,\Psi_y \subset \mathbb{R}$, of identical density λ_w, over the x-axis and the y-axis, respectively. Each realization of Ψ_x and Ψ_y gives rise to a set of points which are considered to be the midpoints of infinite length walls. Hence, the walls grow parallel to the x-axis and the y-axis at every point of these processes and each wall divides the plane into an infinite number of rectangular boxes. Each of these boxes

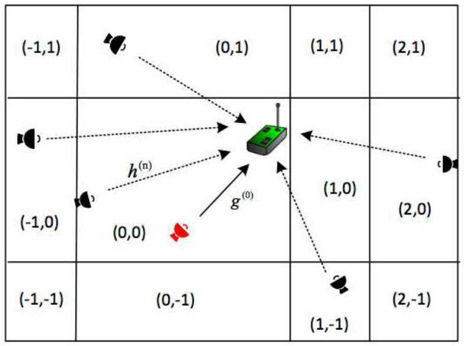

Fig. 2. SWIPT indoor network

is considered as a room of our indoor environment. The room that contains the origin, called typical room, is identified by the couple $(0, 0)$, while the other rooms are labeled according to their position with respect to the typical room, e.g. the signal associated with a PH located in the room (i, j) shall cross $|i|$ walls on the x-axis and $|j|$ walls on the y-axis to reach the typical LPD. It is worth to mention that MPLP does not represent the actual deployment of the walls but it represents a statistic model for spatially correlated shadowing.

III. Performance Analysis

In this section we provide a methodology to study the effects of the blockage objects on the SWIPT performance. Then, we provide an expression for the J-CCDF of information rate and harvested power as a function of the network parameters. An illustration of a SWIPT network in an indoor scenario is shown in Fig. 2, where the serving PH (the red one in Fig. 2) is transmitting data and power towards the typical LPD with power gain $g^{(0)}$ (including MRT, MRC) and the signals, coming from all the PHs, experience Rayleigh fading.

A. Wall Blockage Analysis

The main analytical contribution of this paper is the study of the effect of blockage objects on the SWIPT performance. To achieve this, we first decompose the original PPP, Ψ, with density λ_{PH} into the sum of equivalent inhomogeneous PPPs, Ψ_N. However, the number of walls blocking the signal depends on the position of the PHs. In order to obtain the spatial distribution of the PHs experiencing N blocking objects, the displacement theorem [10, Th. 1.3.9] can be advocated. The density of the original PPP is reduced through the probability $P_N(r,\theta)$ that N walls are experienced at the point defined by the polar coordinates (r, θ). The densities of the processes Ψ_N are therefore given by

$$\lambda_N(r,\theta) = \lambda_{PH} P_N(r,\theta). \tag{2}$$

It is worth recalling that walls are modeled through an MPLP which implies that the number of walls in the intervals $[0, r|\cos(\theta)|]$ and $[0, r|\sin(\theta)|]$ along the x- and y-dimensions, respectively, is a random variable with Poisson distribution. According to the probability of having N events in a given interval for a Poisson distribution, $P_N(r,\theta)$ is given as

$$P_N(r,\theta) = \frac{(\lambda_w r|\cos(\theta)| + \lambda_w r|\sin(\theta)|)^N}{N!} \times \exp\{-(\lambda_w r|\cos(\theta)| + \lambda_w r|\sin(\theta)|)\}. \tag{3}$$

Since the choice of the serving PH is associated with the geometry of both the PHs' spatial distribution and the placement of the walls, the preliminary step enabling the analysis of the performance for the system depicted in Fig. 2 is the characterization of the stochastic properties of the minimum path-loss, $L^{(0)}$, and the multi-user interference, $\mathcal{I}_{MU}$. This will be the objective of the following subsections.

1) Minimum Path Loss: As it has been already mentioned, we assume that the serving PH is the one associated with the minimum path-loss, i.e.

$$L^{(0)} = \min_N \left\{ \min_{n\in\Psi_N} \left\{ l_N(r^{(n)}) \right\} \right\} \tag{4}$$

where n denotes the index of the PHs belonging to the inhomogeneous PPPs associated with N obstacles, Ψ_N, and $r^{(n)}$ is the distance between the device and the nth PH. Following the procedure proposed in [10], we capitalize on the well-known displacement theorem to end up with the following proposition.

Proposition 1: Let the minimum path-loss being the one defined in (4) *and define a function* $\chi_\eta(\lambda_w)$ *as*

$$\chi_\eta(\lambda_w) = \lambda_w^\eta \left[\frac{2^{\frac{\eta}{2}}\sqrt{\pi}\,\Gamma(\frac{\eta+1}{2})}{\Gamma(\frac{\eta+2}{2})} - \frac{\sqrt{2}\,{}_2F_1\left(\frac{1}{2}, \frac{\eta+1}{2}, \frac{\eta+3}{2}, \frac{1}{2}\right)}{\eta+1} \right] \tag{5}$$

where $\Gamma(\cdot,\cdot)$ *is the upper-incomplete Gamma function,* ${}_2F_1(\cdot)$ *is the Gaussian hypergeometric function [19] and* $\eta \in \mathbb{R}_+$ *is a slack variable introduced in Appendix A. Then the cumulative distribution function (CDF) of* $L^{(0)}$ *is given by*

$$F_{L^{(0)}}(\alpha) = \Pr\{L^{(0)} \le \alpha\} = 1 - \prod_{N=0}^{N_{max}} \exp\{-\Lambda_N([0,\alpha))\} \tag{6}$$

where N_{max} *is the number of walls beyond which the attenuation due to blockage makes negligible signal contribution to the rate-energy trade-off.*

$$\Lambda_N([0,\alpha)) = \begin{cases} \dfrac{4\lambda_{PH}}{N!} \displaystyle\sum_{\eta=N}^{\infty} \frac{(-1)^{\eta-N}\chi_\eta(\lambda_w)}{(\eta-N)!(\eta+2)} \left(\frac{\alpha K^N}{\kappa}\right)^{\frac{\eta+2}{\beta}} \\ \quad \text{if } 1 \le \alpha < \dfrac{R_D^\beta \kappa}{K^N} \\ \dfrac{4\lambda_{PH}}{N!} \displaystyle\sum_{\eta=N}^{\infty} \frac{(-1)^{\eta-N}\chi_\eta(\lambda_w)}{(\eta-N)!(\eta+2)} R_D^{\eta+2} \\ \quad \text{if } \alpha \ge \dfrac{R_D^\beta \kappa}{K^N} \end{cases} \tag{7}$$

is the intensity of the process $L_N = \left\{ l_N(r^{(n)}), n \in \Psi_N \right\}$.

Proof: See Appendix A. □

From (7), it is apparent that the signal attenuation is a process whose intensity can be expressed as the weighted

TABLE I
VALUES OF $\chi_\eta(\lambda_w)$

$\lambda_w \backslash \eta$	0	1	2	3	4	5
0.01	1.5708	0.02	2.5×10^{-4}	3.3×10^{-6}	4.35×10^{-8}	5.73×10^{-10}
0.02	1.5708	0.04	1×10^{-3}	2.6×10^{-5}	6.96×10^{-7}	1.83×10^{-8}
0.03	1.5708	0.06	2.3×10^{-3}	9×10^{-5}	3.5×10^{-6}	1.39×10^{-7}
0.04	1.5708	0.08	4.1×10^{-3}	2.1×10^{-4}	1.1×10^{-5}	5.87×10^{-7}
0.05	1.5708	0.1	6.4×10^{-3}	4.1×10^{-4}	2.7×10^{-5}	1.79×10^{-6}

sum of power functions of α. Interestingly, the effects of the blockage due to the walls are captured by the weights $\chi_\eta(\lambda_w)$ that can be computed offline and tabulated for given values of η and λ_w as shown in Table I. Since $\chi_\eta(\lambda_w)$ is a decreasing function of η, from (6) and (7), above a certain number of obstacles which the signal can encounter, the values of $\chi_\eta(\lambda_w)$ become negligible. Consequently, we can infer that the greater the number of obstacles N, the lower the impact of the blockage objects on the CDF of $L^{(0)}$. On the contrary, $\chi_\eta(\lambda_w)$ is an increasing function of λ_w and, not surprisingly, the impact of the blockage objects on $F_{L^{(0)}}(\alpha)$ increases with λ_w.

2) Multi-User Interference: The normalized (with respect to 1W of transmit power) multi-user interference can be expressed as

$$\mathcal{I}_{MU} = \sum_{N=0}^{N_{max}} \sum_{n \in \Psi_N} \frac{h^{(n)}}{l_N(r^{(n)})} \mathbb{1}\left\{l_N(r^{(n)}) > L^{(0)}\right\} \quad (8)$$

where $h^{(n)}$ is an exponentially distributed random variable with unit variance representing the gain of the nth interfering link.

Proposition 2: For a given path-loss $L^{(0)}$, consider the functions $\chi_\eta(\lambda_w)$, $\eta \in \mathbb{R}_+$ as in (5), *and define the function*

$$\begin{aligned}
&\Delta_{\eta,N}\left(\omega; L^{(0)}\right) \\
&= \left(\frac{L^{(0)}K^N}{\kappa}\right)^{\frac{\eta+2}{\beta}} \left(1 - {}_2F_1\left(1, -\frac{\eta+2}{\beta}, 1 - \frac{(\eta+2)}{\beta}, \frac{j\omega}{L^{(0)}}\right)\right) \\
&\quad - R_D^{\eta+2}\left(1 - {}_2F_1\left(1, -\frac{\eta+2}{\beta}, 1 - \frac{(\eta+2)}{\beta}, \frac{j\omega K^N}{R_D^\beta \kappa}\right)\right).
\end{aligned} \quad (9)$$

Then, capitalizing on the Gil-Pelaez inversion theorem, [20], the CDF of $\mathcal{I}_{MU}$ is given by

$$\begin{aligned}
&F_{\mathcal{I}_{MU}}(z; L^{(0)}) \\
&= \Pr\{\mathcal{I}_{MU} \le z | L^{(0)}\} \\
&= 1/2 - \int_0^\infty \frac{1}{\pi\omega} \operatorname{Im}\left\{e^{-j\omega z} \prod_{N=0}^{N_{max}} \Phi_N\left(\omega; L^{(0)}\right)\right\} d\omega
\end{aligned} \quad (10)$$

where $\Phi_N\left(\omega; L^{(0)}\right)$ is the characteristic function of the multi-user interference produced by the PHs whose signals are subject to the attenuation of N obstacles to reach the typical LPD and shown in (11), *shown at the top of the next page.*

Proof: See Appendix B. □

B. SWIPT Performance Analysis

The goal of this section is to provide an analytical expression for studying the stochastic behavior of the SWIPT performance as a function of the PHs' density λ_{PH} and the density of blockage objects λ_w. In view of the multiobjective nature of the system, two different performance metrics are considered, namely the average throughput, expressed in bits/sec and denoted with R, and the average harvested power, measured in Watt and referred to as Q. To achieve this goal, the instantaneous metrics are first defined as

$$\begin{aligned}
R &= B_c \log_2\left(1 + \frac{P g^{(0)}/L^{(0)}}{P\mathcal{I}_{MU} + \sigma_n^2 + \sigma_c^2/(1-\rho)}\right) \\
Q &= \rho\xi P\left(\frac{g^{(0)}}{L^{(0)}} + \mathcal{I}_{MU}\right)
\end{aligned} \quad (12)$$

where B_c is the signal bandwidth, P is the average transmit power, ρ is the power splitting ratio and ξ is the energy harvesting efficiency factor. The variance of the thermal noise is denoted by σ_n^2, while σ_c^2 indicates the variance of the noise due to the conversion of the received signal from radio frequency to baseband [21]. In (12) it is assumed that the harvested power is a linear function of the received power. It is worth mentioning that radio frequency energy harvesters (RFEHs) are in general nonlinear devices, so that the efficiency of the harvesting process would actually depend on the particular SWIPT waveform adopted. However, for the sake of tractability, we make the hypothesis that the system adopts an optimized waveform which provides an almost constant efficiency across all the operating region of the RFEH. In addition to the minimum path-loss $L^{(0)}$ and the multi-user interference $\mathcal{I}_{MU}$, whose statistical properties have been studied in the previous subsections, the other source of randomness is the power gain $g^{(0)}$, which encompasses the small scale fading experienced by the serving PH's signal and the effect of both the MRT and the MRC processing at the transmitter and the receiver side, respectively. As mentioned in [22], the MRT-MRC processing minimizes the induced bit- or symbol- error probability and therefore maximizes the output SNR. This maximization yields to $g^{(0)}$, which is the largest eigenvalue of the Hermitian matrix representing the small scale fading. The PDF of $g^{(0)}$ is therefore given as [22],

$$f_{g^{(0)}}(\zeta) = \mathcal{K}_{m,n} \sum_{s=1}^{m} \sum_{t=n-m}^{(n+m-2s)s} a_{s,t}\zeta^t \exp(-s\zeta) \quad (13)$$

where $m = \min(n_t, n_r)$ and $n = \max(n_t, n_r)$. Here $\mathcal{K}_{m,n} = \prod_{k=1}^{m}((m-k)!(n-k)!)^{-1}$ is a normalizing factor and $a_{s,t}$

$$\Phi_N\left(\omega; L^{(0)}\right) = \begin{cases} \exp\left\{\frac{4\lambda_{PH}}{N!}\sum_{\eta=N}^{\infty}\frac{(-1)^{\eta-N}\chi_\eta(\lambda_w)}{(\eta-N)!(\eta+2)}\Delta_{\eta,N}\left(\omega; L^{(0)}\right)\right\} & \text{if } L^{(0)} < \frac{R_D^\beta \kappa}{K^N} \\ 1 & \text{if } L^{(0)} \geq \frac{R_D^\beta \kappa}{K^N} \end{cases} \tag{11}$$

$$F_c(R^*, Q^*) = \mathbb{E}_{L^{(0)}}\left\{\int_{(\mathcal{T}_*/P)L^{(0)}}^{+\infty} F_{\mathcal{I}_{MU}}\left(x\gamma/L^{(0)} - \sigma_*^2/P \,\middle|\, L^{(0)}\right) f_{g^{(0)}}(x)dx\right\} - \mathbb{E}_{L^{(0)}}\left\{\int_{(\mathcal{T}_*/P)L^{(0)}}^{+\infty} F_{\mathcal{I}_{MU}}\left(-x/L^{(0)} + q_*/P \,\middle|\, L^{(0)}\right) f_{g^{(0)}}(x)dx\right\} \tag{15}$$

$$J_{s,t}^{(1)} = \int_1^\infty\int_0^\infty \frac{1}{\pi w}\,\mathrm{Im}\left\{\exp\left(-jw\frac{q_*}{P}\right)\left(s-\frac{jw}{y}\right)^{-(1+t)}\Gamma\left(1+t, \frac{\mathcal{T}_*}{P}(sy-jw)\right)\Phi(w;y)\right\} \times \left(\widehat{\Lambda}([0,\alpha))\exp\{-\Lambda([0,\alpha))\}\right)dwdy \tag{18}$$

$$J_{s,t}^{(2)} = \int_1^\infty\int_0^\infty \frac{1}{\pi w}\,\mathrm{Im}\left\{\exp\left(jw\frac{\sigma_*^2}{P}\right)\left(s+\frac{jw\gamma}{y}\right)^{-(1+t)}\Gamma\left(1+t, \frac{\mathcal{T}_*}{P}(sy+jw\gamma)\right)\Phi(w;y)\right\} \times \left(\widehat{\Lambda}([0,\alpha))\exp\{-\Lambda([0,\alpha))\}\right)dwdy \tag{19}$$

are some coefficients that can be easily obtained by using [22, Algorithm 1].

In SWIPT-enabled networks the performance of the system can be described in terms of achievable trade-offs between the information rate and the harvested power. This trade-off will be analyzed taking advantage of the J-CCDF of R and Q, as originally proposed in [14]. The J-CCDF is defined as

$$F_c(R^*, Q^*) = \Pr\{R \geq R^*, Q \geq Q^*\} \tag{14}$$

where $Q^* \geq 0$ is the sensitivity of the energy harvester and $R^* \geq 0$ is the minimum desired rate. A convenient reformulation of the J-CCDF has been proposed in [15], and it amounts to computing the probability that the multi-user interference belongs to an interval for which a minimum SINR γ can be achieved conditioned to a minimum amount of received power q_* as given in (15), shown at the top of this page, where $\sigma_*^2 = \sigma_n^2 + \sigma_c^2(1-\rho)^{-1}$, $q_* = Q^*/(\rho\xi)$, $\mathcal{T}_* = (q_* + \sigma_*^2)/(\gamma+1)$ and $\gamma = 1/\left(2^{R^*/B_c} - 1\right)$.

Proposition 3: Let us define,

$$\Phi\left(\omega; L^{(0)}\right) = \prod_{N=0}^{\infty}\Phi_N\left(\omega; L^{(0)}\right),$$
$$\Lambda([0,\alpha)) = \sum_{N=0}^{\infty}\Lambda_N([0,\alpha)), \tag{16}$$

and $\widehat{\Lambda}([0,\alpha))$ as the derivative of $\Lambda([0,\alpha))$ with respect to α, whose expression is provided by (27) *in Appendix B .*

Given the statistical characterization of $L^{(0)}$, $\mathcal{I}_{MU}$, and $g^{(0)}$ expressed as in (6)*,* (29)*, and* (13)*, respectively, the J-CCDF $F_c(R^*, Q^*)$ can be computed as [15],*

$$F_c(R^*, Q^*) = \mathcal{K}_{m,n}\sum_{s=1}^{m}\sum_{t=n-m}^{(n+m-2s)s} a_{s,t}\left(J_{s,t}^{(1)} - J_{s,t}^{(2)}\right) \tag{17}$$

where the functions $J_{s,t}^{(1)}$ and $J_{s,t}^{(2)}$ are defined in (18) *and* (19)*, shown at the top of this page.*

Proof: The proof trivially follows from [15, Proposition 1]. □

Using Proposition 3 the J-CCDF can be numerically computed for illustrating the average trade-off between the information rate and the harvested power without the need of time consuming Monte Carlo simulations.

IV. Numerical Results

In this section, we show the performance for an in-building SWIPT network by means of numerical results. The analytical findings presented in Section III will be validated through Monte Carlo simulations.

A. Setup

We considered a large indoor area with $R_D = 60$m being the maximum distance at which a PH's contribution to the global interference has a non-negligible impact on the achievable rate-energy trade-offs. A set of PHs is transmitting with an average power of 1W, i.e. $P = 30$dBm. The SWIPT signals have a bandwidth of $B_c = 200$kHz centered around $f_c = 2.1$ GHz. The thermal noise has a variance $\sigma_n^2 = -174 + 10\log_{10}(B_c) + \mathcal{F}_n$, where $\mathcal{F}_n = 10$dB is the noise figure. The variance of the noise due to the RF to DC conversion is set to $\sigma_c^2 = -70$dBm. The PHs are assumed to be deployed with a density $\lambda_{PH} = 1/(\pi d_{PH}^2)$, where d_{PH} is half of the average distance between PHs. The efficiency of the RF energy harvesting process is $\xi = 0.8$ and the path-loss exponent is $\beta = 2.5$. Unless otherwise stated, the power splitting factor is $\rho = 0.5$, the number of receive antennas is $n_r = 2$ and the number of transmit antennas is $n_t = 4$. For the chosen

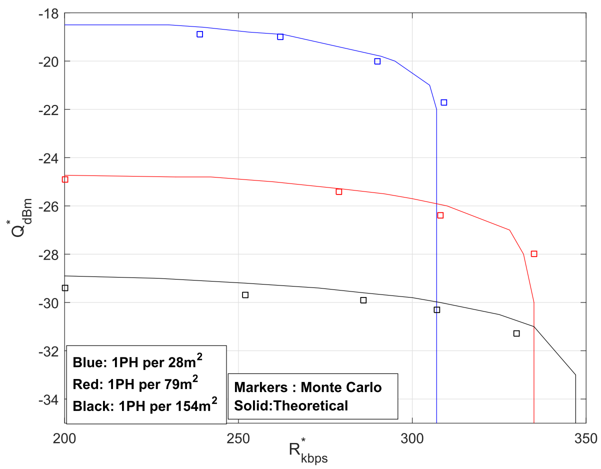

Fig. 3. Monte Carlo simulations and theoretical results of rate-energy trade-off for different λ_{PH} when $\lambda_w = 0.05$, $n_t = 4$, $n_r = 2$.

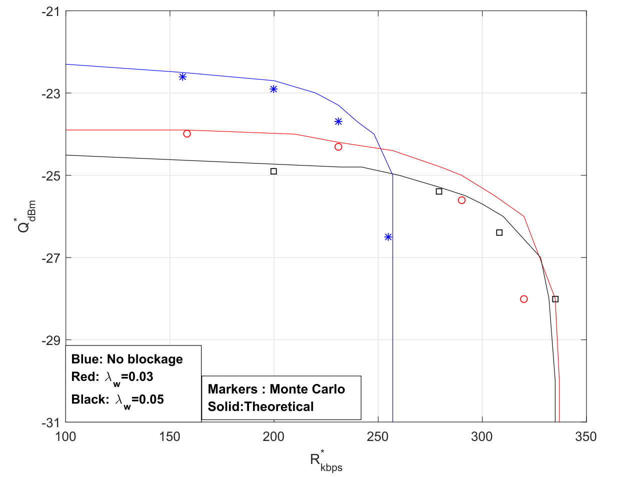

Fig. 4. Monte Carlo simulations and theoretical results of rate-energy trade-off for different λ_w when $d_{PH} = 5m$, $n_t = 4$, $n_r = 2$.

frequency, according to [23, Table 3], the penetration loss K can be reasonably set to -10dB per crossed wall.

B. Results

1) Validation of the Analytical Findings: Fig. 3 shows the trade-off between the information rate and the harvested power parameterized with respect to λ_{PH} when $F_c(R^*, Q^*) = 0.75$. The results are presented for different values of $d_{PH} = 3, 5,$ 7 meters $\left(\text{i.e. } \lambda_{PH} = \frac{1}{28}, \frac{1}{79}, \frac{1}{154}\right)$, while the density of the walls is kept fixed to $\lambda_w = 0.05$. The analytical results (solid lines) are compared to the ones obtained through Monte Carlo simulations (squares). Despite of the approximation due to the fact that the series in (7) and (11) has to be cut at some point, an almost perfect match between theoretical results and simulations is apparent. Clearly, the harvested power always benefits from the increase of the PHs' density λ_{PH}, while the maximum achievable information rate decreases because of the larger level of multi-user interference. We can therefore identify a first compromise to be achieved when the network elements are densified. For example, if a minimum harvested energy of -23dBm is required, the optimum PHs' density is the one corresponding to $d_{PH} = 3$ meters (blue line), while if a harvested energy of -28dBm is sufficient, it would be better to have a less dense network, $d_{PH} = 5$ meters, to benefit from a higher information rate (red line).

In order to investigate the effect of the walls on the SWIPT performance, Monte Carlo simulations (markers) and theoretical results (solid lines) are provided in Fig. 4 when $F_c(R^*, Q^*) = 0.75$ and $d_{PH} = 5$ meters . The blue curve is used as a benchmark and represents the case in which all the blockage objects have been removed. The red and black curves are associated with two different values of λ_w: $\lambda_w = 0.03$ and $\lambda_w = 0.05$, respectively. It is apparent that an increment of the density of blockage objects is beneficial for the maximum achievable information rate because of the reduced multi-user interference. On the other side, we notice a reduction of the harvestable power level when λ_w increases. We can conclude, that the topology of the venue impacts the

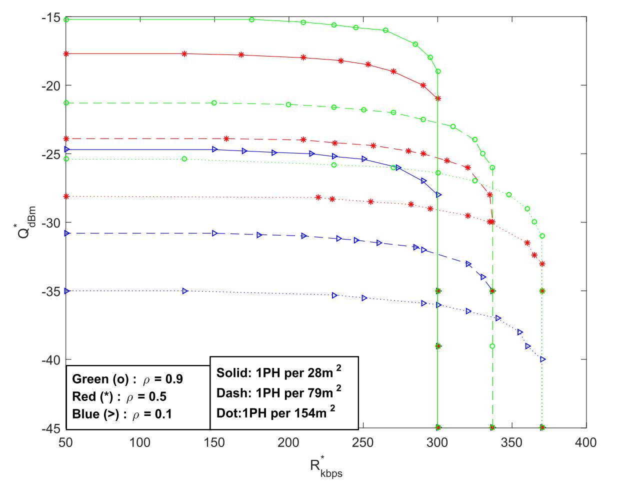

Fig. 5. Theoretical results of rate-energy trade-off for different ρ values when $F_c(R^*, Q^*) = 0.75$, $\lambda_w = 0.03$, $n_t = 4$ and $n_r = 2$.

achievable rate-energy trade-off in view of the ambivalent role of the multi-user interference in SWIPT networks.

2) SWIPT Receiver Analysis: We now analyze the role of the SWIPT receiver architecture on the achievable performance. The rate-energy trade-offs for different values of the power splitting ratio when $F_c(R^*, Q^*) = 0.75$ are presented in Fig. 5. The curves are provided for 3 different values of λ_{PH} when $\lambda_w = 0.03$. Obviously, the receiver harvests more power with higher power splitting ratio for all cases. More interestingly, we obtain the same value of maximum achievable information rate for all values of ρ. This is due to the fact that, with the level of densification required to receive a total power belonging to the microwatt region, the system is essentially interference limited and the SINR does not depend on ρ for realistic levels of noise. For instance, considering the case $d_{PH} = 3m$ (solid lines), with an information rate of 300 Kbps, -27dBm of harvested power can be achieved when $\rho = 0.1$, while we can obtain -20dBm and -17dBm of harvested power when ρ is equal to 0.5 and 0.9, respectively. We can conclude that the power splitting ratio must be as large as possible and its fine tuning is of limited interest in the

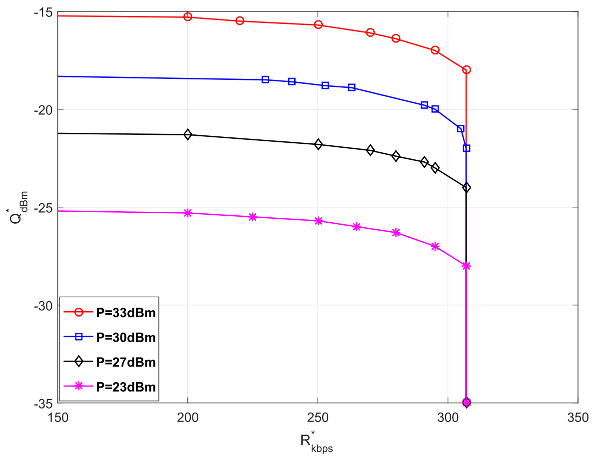

Fig. 6. Theoretical results of rate-energy trade-off for different P values when $F_c(R^*, Q^*) = 0.75$, $d_{PH} = 3$ and $\lambda_w = 0.05$.

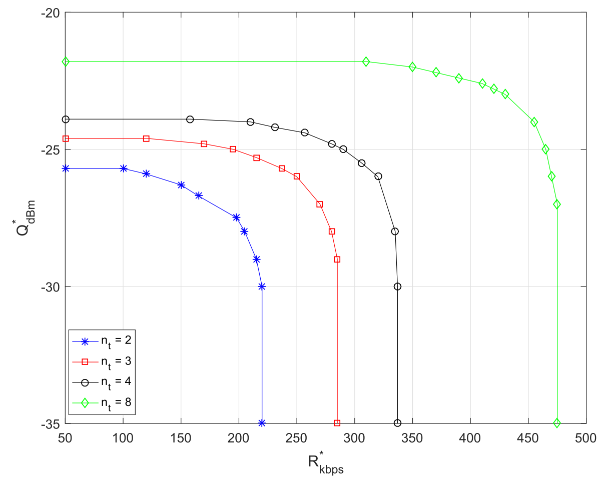

Fig. 7. Theoretical results for rate-energy trade-off as a function of n_t when $n_r = 2$, $\lambda_w = 0.03$ and $d_{PH} = 5m$.

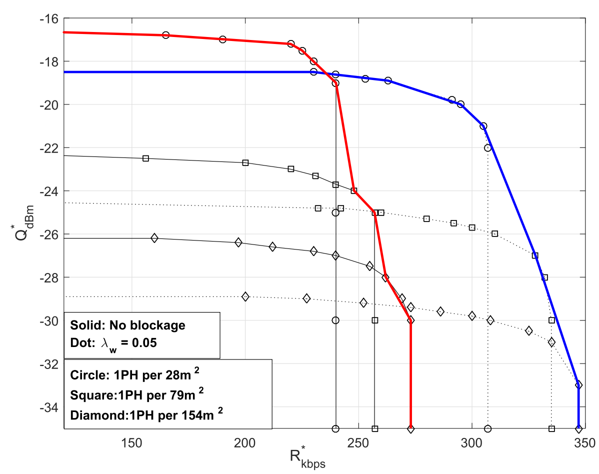

Fig. 8. Theoretical results for the envelope of rate-energy trade-off for different λ_{PH} and λ_w when $F_c(R^*, Q^*) = 0.75$, $n_t = 4$, $n_r = 2$.

design of ultra-dense SWIPT networks. It is worth remarking that this conclusion is radically different from previous works (see [15]) in which the authors consider values of harvested power below -60dBm. In that case, multi-user interference has a limited role while the optimization of the power splitting ratio is paramount. On the contrary, in this paper we show that the technological limitations of the harvesting process make the topology of the venue and its effect on the interference the most important parameters in defining the achievable rate-energy trade-off.

3) Transmit Power Effect Analysis: In order to see the effect of the transmit power, Fig. 6 illustrates the rate-energy trade-off for different values of the transmit power when $n_t = 4$ and $n_r = 2$. As expected, more energy is harvested with higher values of transmit power. However, since the system is interference limited and the SINR is not affected by the change on values of P, the same maximum achievable information rate is obtained for all the considered cases.

4) MIMO Effect Analysis: The previous subsections showed how the ambivalent role of the interference impacts the rate-energy trade-off. On the other side, both harvested energy and information rate can be improved by increasing the power gain from the serving PH to the typical LPD. This can be achieved by increasing the antenna array gain. It is worth mentioning that in this paper we refer exclusively to the rate-energy trade-off of the link while the additional energy consumption required to implement MRC at the LPD is not considered in the performance metrics. In order to illustrate the benefits of MIMO on the SWIPT performance in such a dense interference-limited scenario, Fig. 7 provides the rate-energy trade-off for different numbers of transmit antennas when $F_c(R^*, Q^*)$ is 0.75 and $n_r = 2$. The proposed results show how increasing the number of antennas is of great help in dealing with the MUI while improving the level of harvestable power. Here, for illustrative purposes, we present numerical results only for $\lambda_w = 0.03$, but the same trend has been observed for all the tested densities of walls.

5) Joint Effect of λ_{PH} and λ_w on the Achievable Rate-Energy Trade-Off: Eventually, we focus on how the level of network densification must be wisely chosen in accordance with the topological characteristic of the indoor environment. To this purpose, Fig. 8 shows the envelopes of the rate-energy trade-offs relevant to different values of λ_{PH} and for a J-CCDF equal to 0.75. In particular, the red curve represents a situation in which all blockage objects have been removed, while the blue curve is associated with the presence of walls with density equal to $\lambda_w = 0.05$. It is apparent that the additional attenuation of walls is beneficial for the achievable trade-off and rate. For example, an information rate of 300 Kbps can be achieved with -20dBm of harvested power in the presence of blockages, while this value is reduced to 240 kbps when those obstacles are removed. In Fig. 9 we plotted the rate-energy trade-off for different values of λ_w with $d_{PH} = 3m$ and $d_{PH} = 7m$. In the denser case, the information rate always benefits from the reduced MUI due to the presence of walls. On the contrary, when the network elements are less dense, the blockage experienced by the serving PH is not compensated by the MUI reduction. Hence, neither the harvested power nor the information rate benefits from the interference. Hence, we can argue that the best achievable trade-off is a multidimensional factor in which

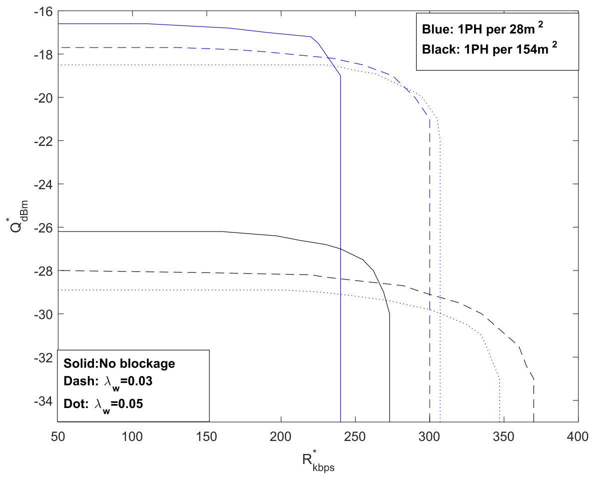

Fig. 9. Theoretical results of rate-energy trade-off for different λ_{PH} and λ_w when $F_c(R^*, Q^*) = 0.75$, $n_t = 4$ and $n_r = 2$.

the cross-dependences between the network infrastructure and the topology of the venue have a major impact.

V. Concluding Remarks

In this paper, we considered a dense in-building MIMO SWIPT network and proposed a stochastic geometry analysis to model the effect of the blocking objects on the SWIPT performance. In this scenario, we addressed the issue of MUI in relation with both the network infrastructure and the topology of the venue. We discovered that there is a nontrivial rate-energy trade-off between the PHs' density and the density of the obstacles. Blockage objects can be beneficial in some cases depending on which trade-off is considered. Their effect in reducing the received power is compensated by the decrease of MUI. Moreover, we investigated the effect of power splitting ratio and transmit power by showing that they have no effect on the maximum achievable information rate while more power can be harvested with their higher values. Finally, it is shown that multi antenna processing is a valuable strategy to counteract the effect of the densification. Our theoretical findings are validated through Monte Carlo simulations.

Appendix A
Proof of Proposition 1

First, we note that the process collecting all the propagation losses $L = \left\{l(r^{(n)}), n \in \Psi\right\}$ can be characterized as a transformation of the points of Ψ. Hence, invoking the displacement theorem, [10, Th. 1.3.9], and recalling that Ψ can be expressed as the superposition of the PPPs Ψ_N, the processes $L_N = \left\{l_N(r^{(n)}), n \in \Psi_N\right\}$, $N \in \{0, N_{max}\}$, are PPPs whose intensity is given by

$$\Lambda_N([0,\alpha)) = \Pr\left\{\frac{\kappa\left(r^{(n)}\right)^{\beta}}{K^N} \in [0,\alpha), n \in \Psi_N\right\} = \lambda_{PH}\int_0^{2\pi}\int_0^{\infty}\mathcal{H}\left(\alpha - \frac{\kappa r^{\beta}}{K^N}\right)P_N\left(r,\theta\right)rdrd\theta. \tag{20}$$

Now, by substituting (3) in (20) and integrating it over r, we get $\Lambda_N([0,\alpha))$ as in (21), shown at the bottom of this page.

In order to have an analytical expression for the integration over the variable θ, we can express the upper-incomplete Gamma functions of θ through their Taylor expansions, i.e.,

$$\Gamma\left(2+N, \left(\frac{\alpha K^N}{\kappa}\right)^{1/\beta}\left(\lambda_w|\cos(\theta)| + \lambda_w|\sin(\theta)|\right)\right) = \Gamma(2+N) - \sum_{i=0}^{\infty}\frac{(-1)^i\left(\frac{\alpha K^N}{\kappa}\right)^{(N+2+i)/\beta}}{i!(i+N+2)} \times \left(\lambda_w|\cos(\theta)| + \lambda_w|\sin(\theta)|\right)^{(N+2+i)}, \tag{22}$$

and

$$\Gamma\left(2+N, R_D\left(\lambda_w|\cos(\theta)| + \lambda_w|\sin(\theta)|\right)\right) = \Gamma(2+N) - \sum_{i=0}^{\infty}\frac{(-1)^i R_D^{(N+2+i)}}{i!(i+N+2)}\left(\lambda_w|\cos(\theta)| + \lambda_w|\sin(\theta)|\right)^{(N+2+i)}, \tag{23}$$

and, substituting (22) and (23) into (21), we get the final expression of $\Lambda_N([0,\alpha))$ as in (24) shown at the top of the next page.

Eventually, it is worth recalling that the Heaviside function is defined as

$$\mathcal{H}(x) = \begin{cases} 1 & \text{if } x \geq 0 \\ 0 & \text{if } x < 0 \end{cases}$$

and that $\bar{\mathcal{H}}(x) = 1 - \mathcal{H}(x)$. Hence, by introducing the slack variable $\eta = N + i$ in (24) and defining the function $\chi_\eta(\lambda_w)$ as in (5), the proof is complete.

$$\Lambda_N([0,\alpha)) = \frac{\lambda_{PH}}{N!}\int_0^{2\pi}\left(\lambda_w|\cos(\theta)| + \lambda_w|\sin(\theta)|\right)^{-2} \times\left[\left(\Gamma(2+N) - \Gamma\left(2+N, \left(\frac{\alpha K^N}{\kappa}\right)^{1/\beta}\left(\lambda_w|\cos(\theta)| + \lambda_w|\sin(\theta)|\right)\right)\right)\bar{\mathcal{H}}\left(\alpha - \frac{R_D^{\beta}\kappa}{K^N}\right) + \left(\Gamma(2+N) - \Gamma\left(2+N, R_D\left(\lambda_w|\cos(\theta)| + \lambda_w|\sin(\theta)|\right)\right)\right)\mathcal{H}\left(\alpha - \frac{R_D^{\beta}\kappa}{K^N}\right)\right]d\theta \tag{21}$$

$$\Lambda_N([0,\alpha)) = \frac{4\lambda_{PH}}{N!}\sum_{i=0}^{\infty}\frac{(-1)^i\lambda_w^{N+i}}{i!(N+i+2)}\left[\frac{2^{\frac{N+i}{2}}\sqrt{\pi}\,\Gamma(\frac{N+i+1}{2})}{\Gamma(\frac{N+i+2}{2})} - \frac{\sqrt{2}\,{}_2F_1\left(\frac{1}{2},\frac{N+i+1}{2},\frac{N+i+3}{2},\frac{1}{2}\right)}{N+i+1}\right] \times \left[R_D^{N+2+i}\ \mathcal{H}\left(\alpha - \frac{R_D^\beta\kappa}{K^N}\right) + \left(\frac{\alpha K^N}{\kappa}\right)^{\frac{N+i+2}{\beta}}\bar{\mathcal{H}}\left(\alpha-\frac{R_D^\beta\kappa}{K^N}\right)\right] \quad (24)$$

$$\Phi_N\left(\omega;L^{(0)}\right) = \exp\left\{\frac{4\lambda_{PH}}{N!}\sum_{\eta=N}^{\infty}\frac{(-1)^{\eta-N}\chi_\eta(\lambda_w)}{(\eta-N)!(\eta+2)}\left[\left(\frac{L^{(0)}K^N}{\kappa}\right)^{\frac{\eta+2}{\beta}}\left(1-{}_2F_1\left(1,-\frac{\eta+2}{\beta},1-\frac{(\eta+2)}{\beta},\frac{j\omega}{L^{(0)}}\right)\right) - R_D^{\eta+2}\left(1-{}_2F_1\left(1,-\frac{\eta+2}{\beta},1-\frac{(\eta+2)}{\beta},\frac{j\omega K^N}{R_D^\beta\kappa}\right)\right)\right]\bar{\mathcal{H}}\left(L^{(0)}-\frac{R_D^\beta\kappa}{K^N}\right)\right\} \quad (28)$$

Appendix B
Proof of Proposition 2

First, let note that the multi-user interference $\mathcal{I}_{MU}$ can be expressed as the sum of the interferences produced by the PHs belonging to Ψ_N, $N \in \{0, N_{max}\}$, where the processes Ψ_N are assumed to be independent. Then, given the minimum propagation loss $L^{(0)}$, the characteristic function of $\mathcal{I}_{MU}$ is given by

$$\Phi\left(\omega;L^{(0)}\right) = \mathbb{E}\left(\exp\left\{j\omega\mathcal{I}_{MU}(L^{(0)})\right\}\right) = \prod_{N=0}^{N_{max}}\Phi_N\left(\omega;L^{(0)}\right) \quad (25)$$

where $\Phi_N\left(\omega;L^{(0)}\right)$ is the characteristic function of the interference generating from the PHs associated with Ψ_N.

In order to compute $\Phi_N\left(\omega;L^{(0)}\right)$, we can invoke the Probability Generating Functional (PGFL) theorem for PPPs (see [10, Proposition 1.2.2]), thus getting

$$\Phi_N\left(\omega;L^{(0)}\right) = \exp\left(\mathbb{E}_{h^{(n)}}\left\{\int_{L^{(0)}}^{\infty}\left(\exp\left(j\omega h^{(n)}/\alpha\right)-1\right)\widehat{\Lambda}_N([0,\alpha))d\alpha\right\}\right) \quad (26)$$

where $\widehat{\Lambda}_N([0,\alpha))$ is the first derivative of $\Lambda_N([0,\alpha))$ with respect to α, given by

$$\widehat{\Lambda}_N([0,\alpha)) = \begin{cases} \dfrac{4\lambda_{PH}}{N!}\dfrac{K^N}{\kappa\beta}\displaystyle\sum_{\eta=N}^{\infty}\dfrac{(-1)^{\eta-N}\chi_\eta(\lambda_w)}{(\eta-N)!}\left(\dfrac{\alpha K^N}{\kappa}\right)^{\frac{\eta+2}{\beta}-1} \quad \text{if } 1 \le \alpha < \dfrac{R_D^\beta\kappa}{K^N} \\ 0 \quad \text{if } \alpha \ge \dfrac{R_D^\beta\kappa}{K^N} \end{cases} \quad (27)$$

with $\chi_\eta(\lambda_w)$ defined as in (5).

Hence, similarly to what has been done in [14], we can use the notable result

$$\int_{\mathcal{N}}^{+\infty}\left(\exp\{j\omega\mathcal{A}/x\}-1\right)x^{v-1}dx = (1/v)\mathcal{N}^v\left(1-{}_1F_1\left(-v,1-v,j\omega\mathcal{A}/\mathcal{N}\right)\right)$$

and compute the expectation with respect to $h^{(n)}$ by taking advantage of the identity in [19, eq. 7.521]. After some manipulations, the expression of the characteristic function is given in (28), shown at the top of this page.

Then, invoking the Gil-Pelaez inversion theorem

$$F_{\mathcal{I}_{MU}}(z;L^{(0)}) = 1/2 - \int_0^\infty \frac{1}{\pi\omega}\,\mathrm{Im}\left\{\mathrm{e}^{-j\omega z}\Phi\left(\omega;L^{(0)}\right)\right\}d\omega, \quad (29)$$

and recalling (9) and (25), Proposition 2 is finally proven.

References

[1] L. R. Varshney, "Transporting information and energy simultaneously," in *Proc. IEEE Int. Symp. Inf. Theory (ISIT)*, Jul. 2008, pp. 1612–1616.

[2] R. Zhang and C. K. Ho, "MIMO broadcasting for simultaneous wireless information and power transfer," *IEEE Trans. Wireless Commun.*, vol. 12, no. 5, pp. 1989–2001, May 2013.

[3] J. G. Andrews, F. Baccelli, and R. K. Ganti, "A tractable approach to coverage and rate in cellular networks," *IEEE Trans. Commun.*, vol. 59, no. 11, pp. 3122–3134, Nov. 2011.

[4] M. Di Renzo, A. Guidotti, and G. E. Corazza, "Average rate of downlink heterogeneous cellular networks over generalized fading channels: A stochastic geometry approach," *IEEE Trans. Commun.*, vol. 61, no. 7, pp. 3050–3071, Jul. 2013.

[5] L. Liu, R. Zhang, and K.-C. Chua, "Wireless information transfer with opportunistic energy harvesting," *IEEE Trans. Wireless Commun.*, vol. 12, no. 1, pp. 288–300, Jan. 2013.

[6] G. Zheng, I. Krikidis, C. Masouros, S. Timotheou, D.-A. Toumpakaris, and Z. Ding, "Rethinking the role of interference in wireless networks," *IEEE Commun. Mag.*, vol. 52, no. 11, pp. 152–158, Nov. 2014.

[7] A. D. Wyner, "Shannon-theoretic approach to a Gaussian cellular multiple-access channel," *IEEE Trans. Inf. Theory*, vol. 40, no. 6, pp. 1713–1727, Nov. 1994.

[8] V. H. M. Donald, "Advanced mobile phone service: The cellular concept," *Bell System Tech. J., The*, vol. 58, no. 1, pp. 15–41, Jan. 1979.

[9] X. Zhang, F. Baccelli, and R. W. Heath, Jr., "An indoor correlated shadowing model," in *Proc. IEEE Global Commun. Conf. (GLOBECOM)*, Dec. 2015, pp. 1–7.

[10] F. Baccelli *et al.*, "Stochastic geometry and wireless networks, part I: Theory," *Found. Trends Netw.*, vol. 3, nos. 3–4, pp. 249–449, 2009.

[11] I. Krikidis, "Simultaneous information and energy transfer in large-scale networks with/without relaying," *IEEE Trans. Commun.*, vol. 62, no. 3, pp. 900–912, Mar. 2014.

[12] X. Zhou, J. Guo, S. Durrani, and I. Krikidis, "Performance of maximum ratio transmission in ad hoc networks with SWIPT," *IEEE Wireless Commun. Lett.*, vol. 4, no. 5, pp. 529–532, Oct. 2015.

[13] X. Lu, I. Flint, D. Niyato, N. Privault, and P. Wang, "Performance analysis of simultaneous wireless information and power transfer with ambient RF energy harvesting," in *Proc. IEEE Wireless Commun. Netw. Conf. (WCNC)*, Mar. 2015, pp. 1303–1308.

[14] W. Lu, M. Di Renzo, and T. Q. Duong, "On stochastic geometry analysis and optimization of wireless-powered cellular networks," in *Proc. IEEE Global Commun. Conf. (GLOBECOM)*, Dec. 2015, pp. 1–7.

[15] T. L. Thanh, M. Di Renzo, and J. P. Coon, "MIMO cellular networks with simultaneous wireless information and power transfer," in *Proc. IEEE 17th Int. Workshop Signal Process. Adv. Wireless Commun. (SPAWC)*, Jul. 2016, pp. 1–5.

[16] T. Bai, R. Vaze, and R. W. Heath, Jr., "Analysis of blockage effects on urban cellular networks," *IEEE Trans. Wireless Commun.*, vol. 13, no. 9, pp. 5070–5083, Sep. 2014.

[17] F. Baccelli and X. Zhang, "A correlated shadowing model for urban wireless networks," in *Proc. IEEE Conf. Comput. Commun. (INFOCOM)*, Apr./May 2015, pp. 801–809.

[18] M. K. Müller, M. Taranetz, and M. Rupp, "Analyzing wireless indoor communications by blockage models," *IEEE Access*, vol. 5, pp. 2172–2186, 2017.

[19] I. S. Gradshteyn and I. M. Ryzhik, *Table of Integrals, Series and Products*. New York, NY, USA: Academic, 2014.

[20] J. Gil-Pelaez, "Note on the inversion theorem," *Biometrika*, vol. 38, pp. 481–482, Dec. 1951.

[21] X. Zhou, R. Zhang, and C. K. Ho, "Wireless information and power transfer: Architecture design and rate-energy tradeoff," *IEEE Trans. Commun.*, vol. 61, no. 11, pp. 4754–4767, Nov. 2013.

[22] A. Maaref and S. Aïssa, "Closed-form expressions for the outage and ergodic Shannon capacity of MIMO MRC systems," *IEEE Trans. Commun.*, vol. 53, no. 7, pp. 1092–1095, Jul. 2005.

[23] *Propagation Data and Prediction Methods for the Planning of Indoor Radiocommunication Systems and Radio Local Area Networks in the Frequency Range 900 MHz to 100 GHz*, document Rec. P.1238, ICU, Geneva, Switzerland, 2012.

Ayse Ipek Akin received the B.Sc. degree in electronic engineering from Gebze Institute of Technology, Kocaeli, Turkey, in 2011, and the M.Sc. degree in telecommunication engineering from Yildiz Technical University, Istanbul, Turkey, in 2013. She is currently pursuing the Ph.D. degree with the Institute of Information and Communication Technologies, Electronics and Applied Mathematics, Université catholique de Louvain, Louvain-La-Neuve, Belgium. Her research interests are cooperative communication, MIMO, relay selection, wireless power transfer, and stochastic geometry and its applications in simultaneous wireless information and power transfer networks.

Ivan Stupia received the M.S. degree in telecommunications engineering and the Ph.D. degree in information engineering from the University of Pisa, Italy, in 2004 and 2009, respectively. In 2011, he joined the Institute of Information and Communication Technologies, Electronics and Applied Mathematics, Université catholique de Louvain. His expertise and general interests span the areas of wireless communications and signal processing with special emphasis on the application of game theory and multiobjective optimization to the design of self-adaptive and self-organizing networks. His current research topic focuses on the analysis of self-sustainable wireless ecosystems with limited computation capability.

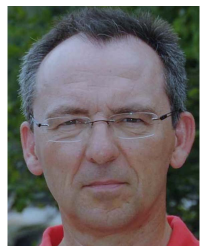

Luc Vandendorpe (M'93–SM99–F'06) was born in Mouscron, Belgium, in 1962. He received the degree *(summa cum laude)* in electrical engineering and the Ph.D. degree from the Université Catholique de Louvain (UCL), Louvain La Neuve, Belgium, in 1985 and 1991, respectively. Since 1985, he has been with the Communications and Remote Sensing Laboratory, UCL, where he first involved in the field of bit rate reduction techniques for video coding. In 1992, he was a Visiting Scientist and a Research Fellow with the Telecommunications and Traffic Control Systems Group, Delft Technical University, The Netherlands, where he was involved in spread spectrum techniques for personal communications systems. From 1992 to 1997, he was a Senior Research Associate of the NSF Belgian, UCL, where he was also an invited Assistant Professor. He is currently a Full Professor with the Institute for Information and Communication Technologies, Electronics and Applied Mathematics, UCL. His research interests include digital communication systems and more precisely resource allocation for OFDM(A)-based multicell systems, MIMO and distributed MIMO, sensor networks, UWB-based positioning, and wireless power transfer.

He was an elected member of the Signal Processing for Communications Committee from 2000 to 2005 and the Sensor Array and Multichannel Signal Processing Committee, Signal Processing Society, from 2006 to 2008 and from 2009 to 2011. He is currently a TPC Member for numerous IEEE conferences, including VTC, Globecom, SPAWC, ICC, PIMRC, and WCNC. He was the Chair of the IEEE Benelux Joint Chapter on communications and vehicular technology from 1999 to 2003. He was the Co-Technical Chair of the IEEE ICASSP 2006. He served as an Editor for Synchronization and Equalization of the IEEE TRANSACTIONS ON COMMUNICATIONS from 2000 to 2002 and an Associate Editor for the IEEE TRANSACTIONS ON WIRELESS COMMUNICATIONS from 2003 to 2005 and the IEEE TRANSACTIONS ON SIGNAL PROCESSING from 2004 to 2006.